Nuclear Physics **A496** (1989) 189-204
North-Holland, Amsterdam

ELASTIC SCATTERING OF POLARIZED PROTONS BY ^{6}Li* (I). Optical-model analysis

M. HALLER, M. BETZ, W. KRETSCHMER, A. RAUSCHER, R. SCHMITT[1] and W. SCHUSTER

Tandemlabor der Universität Erlangen-Nürnberg, Erlangen, Fed. Rep. Germany

Received 9 August 1988
(Revised 20 December 1988)

Abstract: The differential cross sections and the analyzing power for the ^{6}Li(p, p) elastic scattering were measured over the proton laboratory-energy range from 1.6 to 10 MeV (σ) and from 2.8 to 10 MeV (A). The data are well described by optical-model calculations, only if the geometrical parameters are allowed to depend strongly on the energy. The magnitudes of the volume integrals and the root mean square radii are in good agreement with predictions of microscopic theories. Nevertheless, there are resonant structures in the energy dependence of these parameters as well as in the experimental excitation functions. They correspond to a well known resonance at $E_{c.m.} = 1.6$ MeV and to a broad resonance structure at $E_{c.m.} = 4$ MeV, which may be identified as a superposition of resonances recently predicted by refined resonating-group calculations.

E | NUCLEAR REACTIONS ^{6}Li(polarized p, p); $E = 1.6$-10 MeV; measured $\sigma(E, \theta)$, $A(E, \theta)$; deduced optical-model parameters. Enriched target.

1. Introduction

Since some years, the $A = 7$ mirror nuclei ^{7}Be and ^{7}Li have been the object of many experimental and theoretical investigations. Besides the general interest in developing nuclear models for the structure of these nuclei, there are special reasons: The reaction ^{6}Li(n, t)^{4}He is the dominant breeding process for tritium in fusion reactors, and the capture ^{3}He(α, γ)^{7}Be is part of the pp cycle and a key reaction for the understanding of the solar neutrino problem [1]).

Due to the difficulties of direct experimental studies at the very small energies of interest, it is important to develop a microscopic model for the structure of ^{7}Be and ^{7}Li, which describes the experimental thresholds and resonances in a wide energy range. This has been done by Hofmann *et al.* [2,3]) in the framework of refined multichannel and multistructure resonating-group calculations, which predicted some additional resonances near 10 MeV excitation energy in ^{7}Be. Some of these predicted resonances with $J^\pi = \frac{1}{2}^-, \frac{3}{2}^-$ or $\frac{5}{2}^-$, and $T = \frac{1}{2}$, should be found in the elastic

* Supported by the Deutsche Forschungsgemeinschaft.
[1] Present address: FAG Kugelfischer, Erlangen, Fed. Rep. Germany.

scattering of protons at ^{6}Li. Measurements of this reaction may serve as a test for the theoretical resonating-group calculations.

Usually, the optical model formalism is applied to scattering processes, which are dominated by the direct reaction mechanism, i.e. mainly for heavy target nuclei and medium energies. As recently suggested by Dave and Gould in an investigation of unpolarized neutron scattering cross sections [4]), the optical model application may be extended to small mass numbers and small energies, even if broad resonances are present. Another interesting question is, whether the predictions of microscopic models [5]), which are originally designed for large mass numbers, agree with the results of optical-model calculations for ^{6}Li(p, p) scattering. If there are resonances, they should influence the results of the optical-model calculations, which will be discussed in the following sections. More detailed examination of the resonance parameters can be achieved by a complicated phase-shift analysis, which is subject of the subsequent paper.

2. The experiment

Since the amount of existing polarized data was very poor, we measured complete angular distributions (laboratory angles between 30° and 165° in steps of 5°) of the differential cross section and the analyzing power of ^{6}Li(p, p) scattering in a wide lab-energy range (1.6–10 MeV and 2.8–10 MeV, respectively) and in small steps (200 keV steps below 3 MeV, 100 keV steps between 3 and 6 MeV, 500 keV steps above 6 MeV). The measurements were carried out at the Erlangen Tandem accelerator facility. The polarized proton beam was produced by a Lamb-shift type ion source, accelerated by an EN Tandem and focussed into a 4π scattering chamber, which is shown in fig. 1. A long collimator, consisting of a scattering and an antiscattering diaphragm of 3.0 and 3.2 mm diameter, respectively, guided the beam to the exchangeable target. Sixteen surface-barrier detectors were mounted in steps of 10° on two rotatable rings, which were turned by 5° between two runs. In this way, 28 scattering angles between 30° and 165° in steps of 5° could be measured in two runs, with overlaps at 90° and 95°. Collimators in front of each detector limited their solid angles to values between 0.012 msr (30°) and 0.15 msr (160°); thus compensating the increase of the cross section at forward angles. Target current and beam polarization were measured on-line by a combination of ^{4}He polarimeter and Faraday cup at the exit of the scattering chamber. The polarization was switched from up to down every 10 seconds, and the digitized beam current was accumulated and stored separately for each spin orientation. The beam current accumulation was stopped during the dead time of the corresponding ADC.

Special difficulties arose from the target preparation, because Li is hygroscopic and forms quickly Li_2O and LiOH in the air. Initially, LiF on a backing of Ni was used, which caused problems because of interfering lines from inelastic scattering at F and Ni. These lines could be removed by using a sandwich target

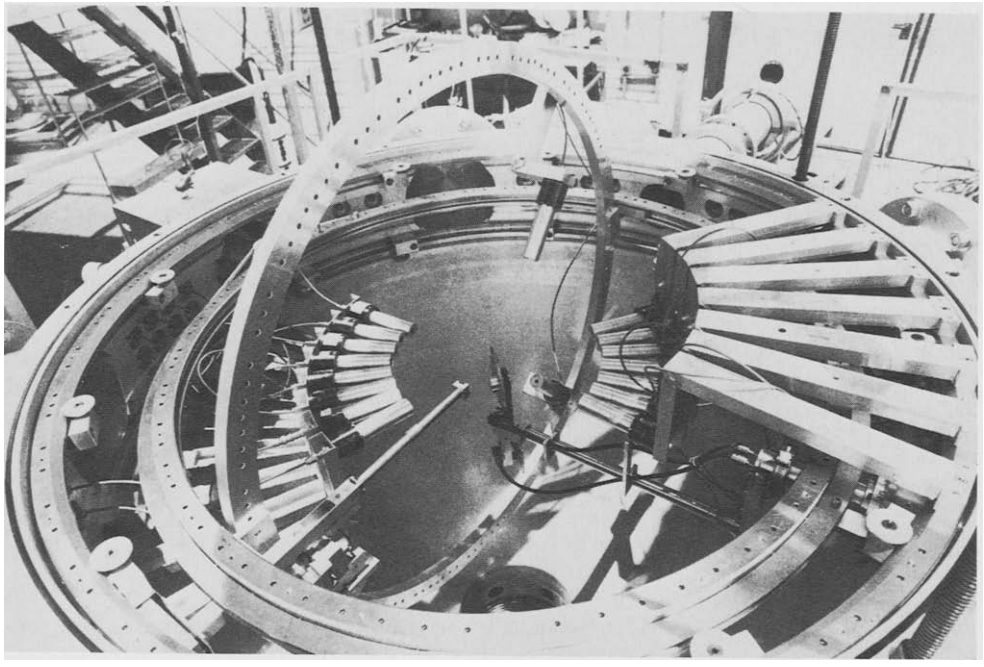

Fig. 1. View from above into the 4π scattering apparatus.

Al-^{6}Li-C, and, with further improvement, C-^{6}Li-C. With this latter kind of target (50 μg/cm^2 ^{6}Li), which had to be stored in vacuum, very clean spectra were obtained, as can be seen in fig. 2. The ^{1}H and ^{16}O background lines result from air moisture, which had penetrated through the very thin and porous carbon backings.

The transmission through the Tandem accelerator decreases at small energies. Below 2.8 MeV proton energy, only the larger beam current of the unpolarized ion source was sufficient. So at these small energies between 1.6 and 2.6 MeV only cross-section measurements have been performed. The polarized beam had a constant (within $\pm 1\%$) polarization of typically 68%. Angle-dependent normalization factors, which depend primarily on the different solid angles of the detectors, were determined by elastic scattering of a low energy (3.4 MeV) proton beam at a thin Au target. This scattering cross section is well described by the Rutherford formula. Normalization errors and systematic errors, arising from spin correlated flipping of the beam axis, were estimated to be small compared with the statistical errors which include the errors from background subtraction in the spectra. As the exact determination of the target thicknesses of the ^{6}Li targets was not practicable, we got the overall normalization of the absolute cross section by adjusting our data between 1.8 and 2.8 MeV to corresponding data of McCray [6]. The data of ref. [6]) include

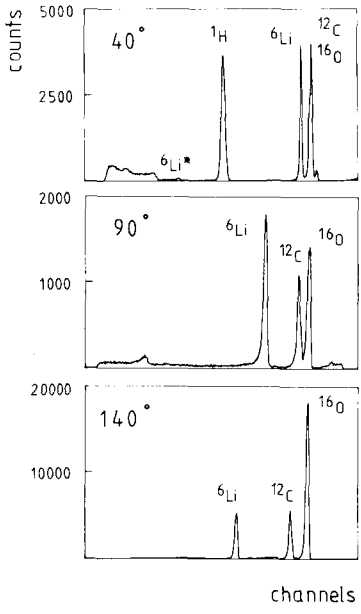

Fig. 2. Spectra of 4 MeV protons, scattered at a C-^{6}Li-C target at laboratory angles 40°, 90° and 140°.

very small energies ($E \geq 0.4$ MeV), and therefore are well described by the Rutherford formula, at least at forward angles. This is not the case for our data starting at $E = 1.6$ MeV. Taking into account an overall normalization error of 5% given in ref. [6]), we determined a 7% overall normalization error for our cross section data.

The angular distributions of the data are compared with optical-model (see sect. 3) and phase-shift calculations (see the following paper). Some insight into resonance structures can be obtained from excitation functions, which are displayed in fig. 3. The differential cross section shows a peak below 2 MeV, which has already been analyzed, for example by McCray [6]), and assigned to be a $\frac{5}{2}^-$ resonance. A broader structure appears at 4–5 MeV and indicates additional resonances, which have been suggested by recent resonating-group calculations [3]). Very similar is the shape of the total elastic cross section (without Rutherford scattering), which is shown in fig. 4. It has been calculated in a phase-shift analysis, which fitted all experimental data.

3. Analysis of the data

In this work the following ansatz for the optical potential was used:

$$V(r) = V_C(r) - V_0 f(r, r_0, a_0) + 4a_I W_D \frac{\mathrm{d}}{\mathrm{d}r} f(r, r_I, a_I) + 2V_{s.o.} \boldsymbol{\sigma} \cdot \boldsymbol{l} \frac{1}{r} \frac{\mathrm{d}}{\mathrm{d}r} f(r, r_{s.o.}, a_{s.o.}),$$

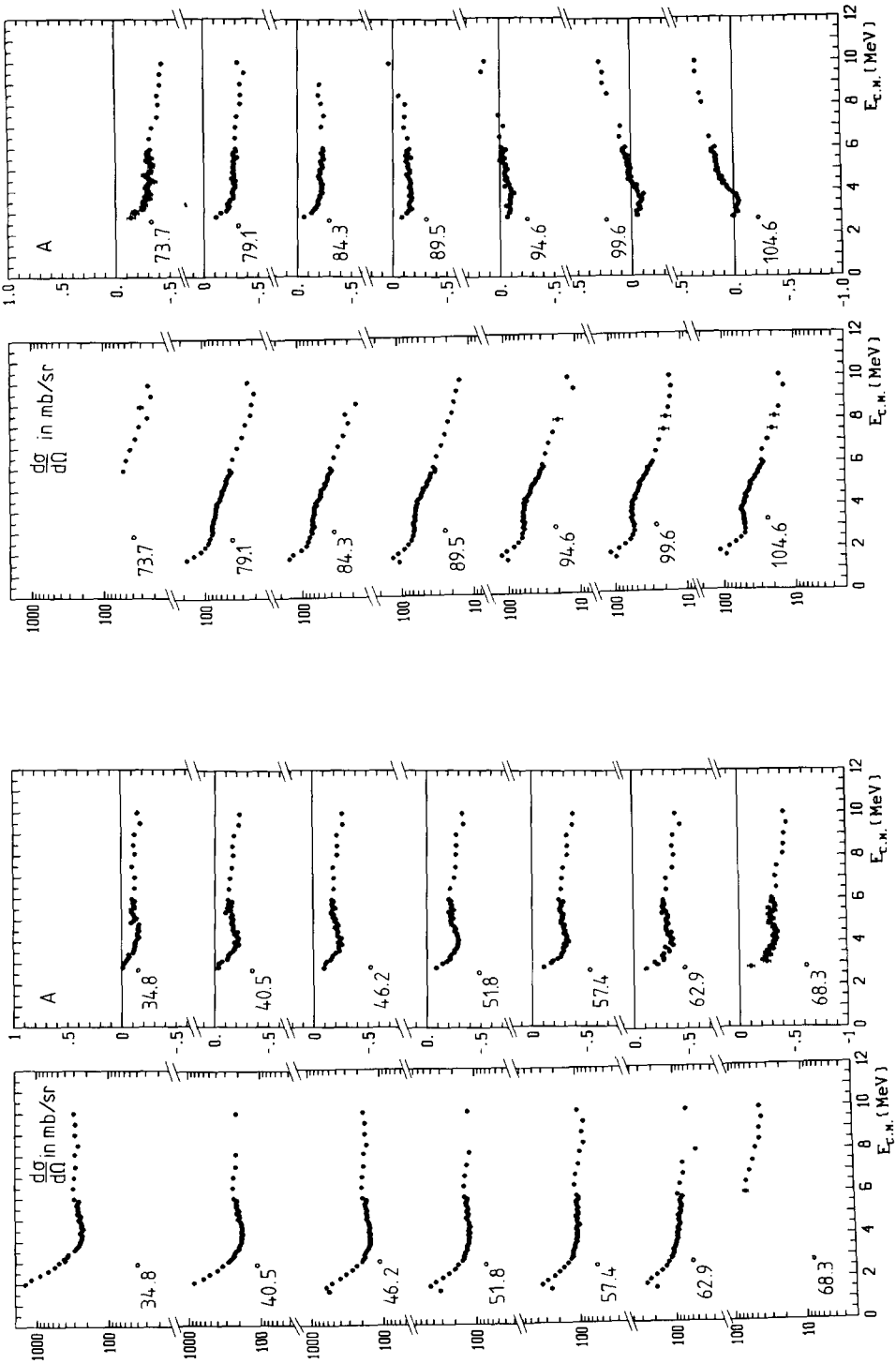

Fig. 3. Cross section and analyzing-power excitation functions for all experimental scattering angles (all values in the c.m. system).

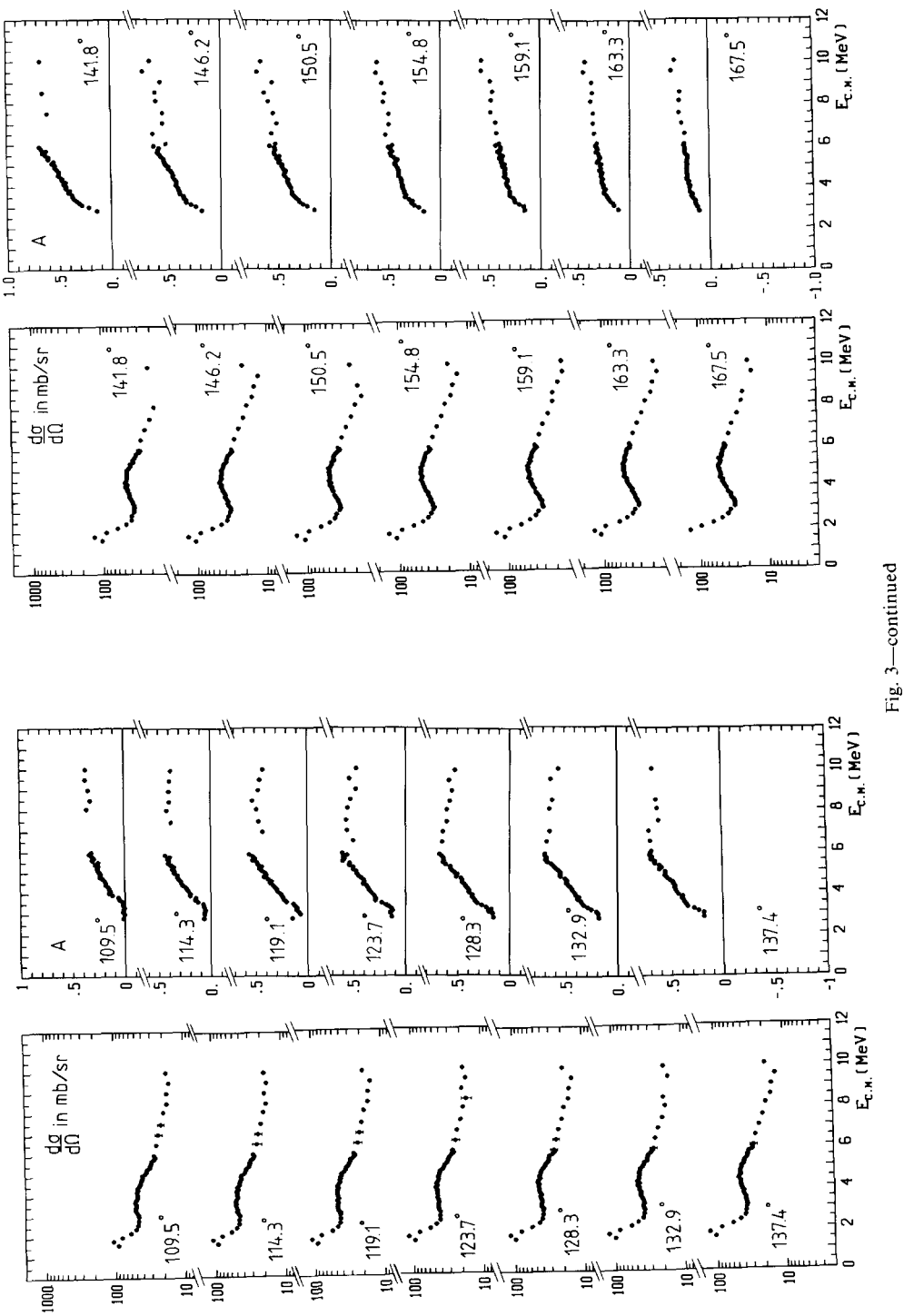

Fig. 3—continued

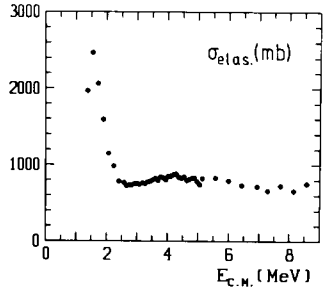

Fig. 4. Total elastic cross section without Coulomb interaction, calculated within a phase-shift analysis fitting all experimental cross section and analyzing power data.

where f is the normal Woods-Saxon form factor

$$f(r, r_x, a_x) = [1 + \exp(r - r_x A^{1/3})/a_x]^{-1}.$$

The Coulomb-potential $V_C(r)$ corresponds to the potential of a homogeneously charged full sphere with the radius $r_C A^{1/3}$; V_0, W_D and $V_{s.o.}$ are the depths of the real, imaginary, and spin-orbit potential, respectively. The spin-spin interaction, which is comparatively small and has little influence on σ and A, has been neglected. In general, the imaginary part of the optical potential consists of a volume and a surface term. The former has been omitted here, because at energies far below 30 MeV only absorption at the nuclear surface is important. Also an imaginary part of the spin-orbit potential turned out to be unimportant for ^{6}Li(p, p) scattering as well as in other earlier analyses of proton scattering (e.g. ref. [7])). In the case of low energy scattering on heavy target nuclei one usually calculates the compound nucleus contributions within the Hauser-Feshbach formalism. This procedure is not applicable to the light nucleus ^{6}Li, because of its small level density; i.e. there are not enough levels within the energy resolution of the experiment and thus the usual statistical assumptions are not valid. In the absence of resonances the observables are described by an optical potential with an only weakly energy-dependent parameter set. If, however, resonances are present, a good description of all observables can probably be only achieved with strongly energy-dependent parameters.

First the data were fitted for each energy separately, using the resulting parameters as starting values for the subsequent energy. The computer code GOMEL [8]) was used, which also calculates errors of the parameters, according to a 10% increase of the χ^2 type error function, and the correlation coefficients between them. In this first fitting procedure (I) the following parameters were kept fixed to avoid ambiguities: $r_C = 1.25$ fm, $r_0 = 1.20$ fm, $a_I = 0.40$ fm, $a_{s.o.} = 0.40$ fm. The other parameters were fitted simultaneously, with the exception of $V_{s.o.}$ and $r_{s.o.}$, which were kept fixed below 2.8 MeV, since at these energies only cross-section data, to which the spin-orbit parameters are not sensitive, have been measured.

The resulting description of the data, as shown in fig. 5 (solid curves), is quite good; there is only a slight discrepancy in the analyzing power in the forward angular region at energies below 5 MeV, where resonances are predicted (compare the discussion of the excitation functions at the end of sect. 2).

The resulting fit parameters of procedure (I) are shown in fig. 6 as function of c.m. energy. Below 3 MeV a resonance structure is seen in all but the (fixed) spin-orbit parameters. It corresponds to the 1.6 MeV resonance in the excitation functions discussed above. The value of the spin-orbit potential is larger than usual, but it was not possible to describe the data with a significantly smaller value. The real potential increases with energy, whereas the usual behaviour is a slight decrease [9]). An attempt to fit the data in the usual way with linearly energy-dependent optical-model parameters was performed in procedure (II), where $\sigma(\theta)$ and $A(\theta)$ for $E_{lab} = 3, 5, 7$, and 9 MeV were analyzed simultaneously. To avoid ambiguities, the parameters were varied alternatingly over several fit runs. The resulting parameters are listed in table 1, and the description of the data is shown in fig. 7. It is of course not as good as from procedure (I), especially at very small energies, but the energy dependence of the potential depths is much more reasonable.

Therefore, in a third procedure (III) the potential depths V_0, W_D, $V_{s.o.}$ and imaginary potential diffuseness a_I were kept fixed with the appropriate values according to table 1. The remaining free parameters r_0, a_0, r_I, $r_{s.o.}$, $a_{s.o.}$ were fitted analogously to procedure (I), leading to a similarly good description of the data as shown in fig. 5 (dashed curves). Only at the smallest energies there are some discrepancies, probably resulting from the constant V_0, compared with its strong structure in procedure (I) (see fig. 6). The varied parameters of procedure (III) are plotted in fig. 8. Similarly to the results of procedure (I) (fig. 6), there are structures which correspond well to the resonance in the total cross section (fig. 4), especially r_I, which is narrower than before. These structures appear independently from the special fitting procedure applied. It was not possible to describe both cross section and analyzing power, if the geometry parameters were not allowed to vary strongly with energy. We may conclude that there are energy regions where due to the presence of compound-nucleus resonances, a proper description of the data is not possible with a weakly energy-dependent optical potential. This is not the case, as has been shown in ref. [4]), if only unpolarized cross-section data are analyzed.

4. Volume integrals and root mean square radii

For a comparison of different analyses of experimental data or theoretical predictions, usually volume integrals and root mean square (r.m.s.) radii are considered. In this way parameter ambiguities (V_{r^2} and Wa_I) and the influence of the special radial dependences of the form factors are drastically reduced. These quantities are defined as follows:

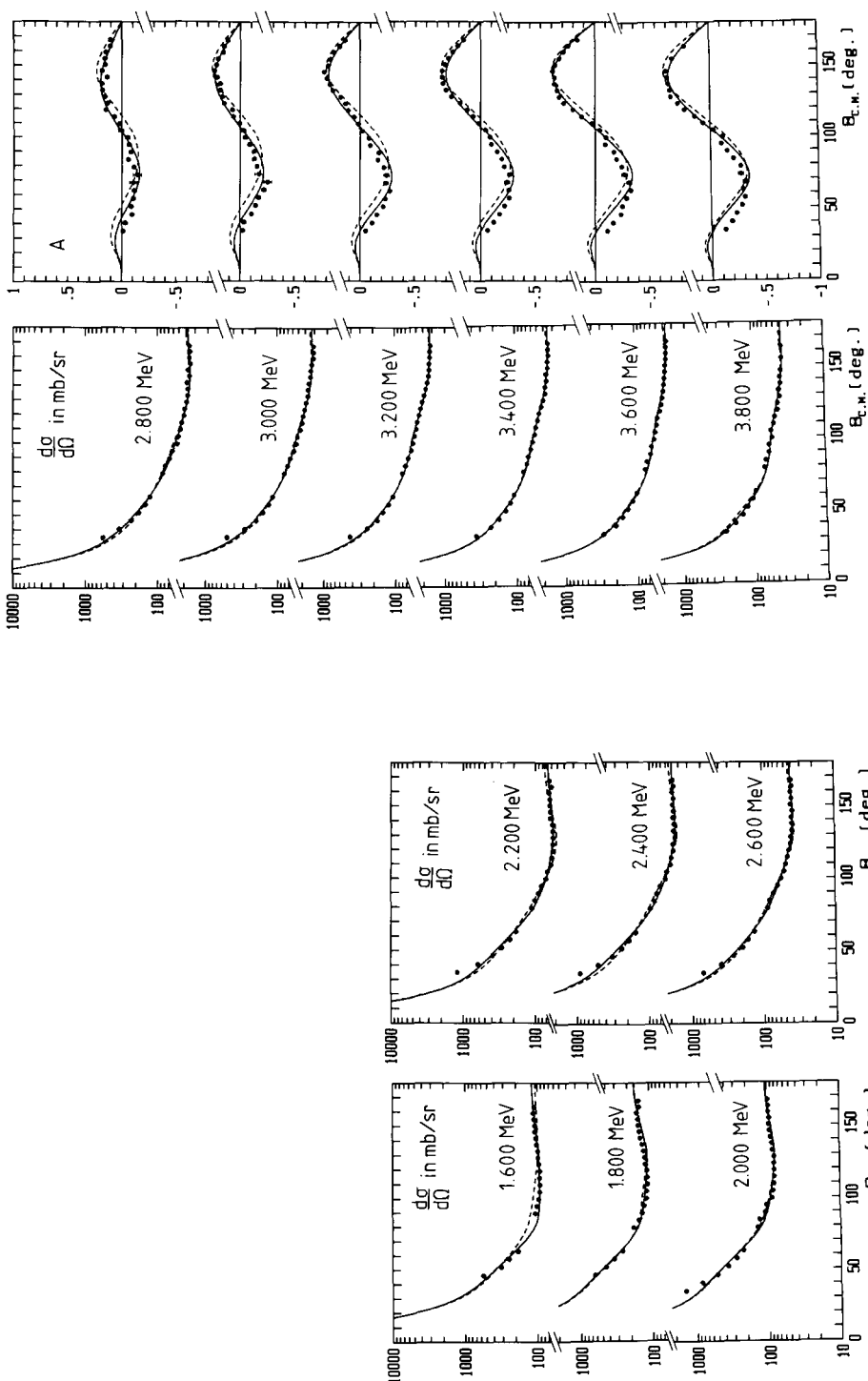

Fig. 5. Description of experimental data within the optical model by procedure (I) (solid curves) and (III) (dashed curves), see text.

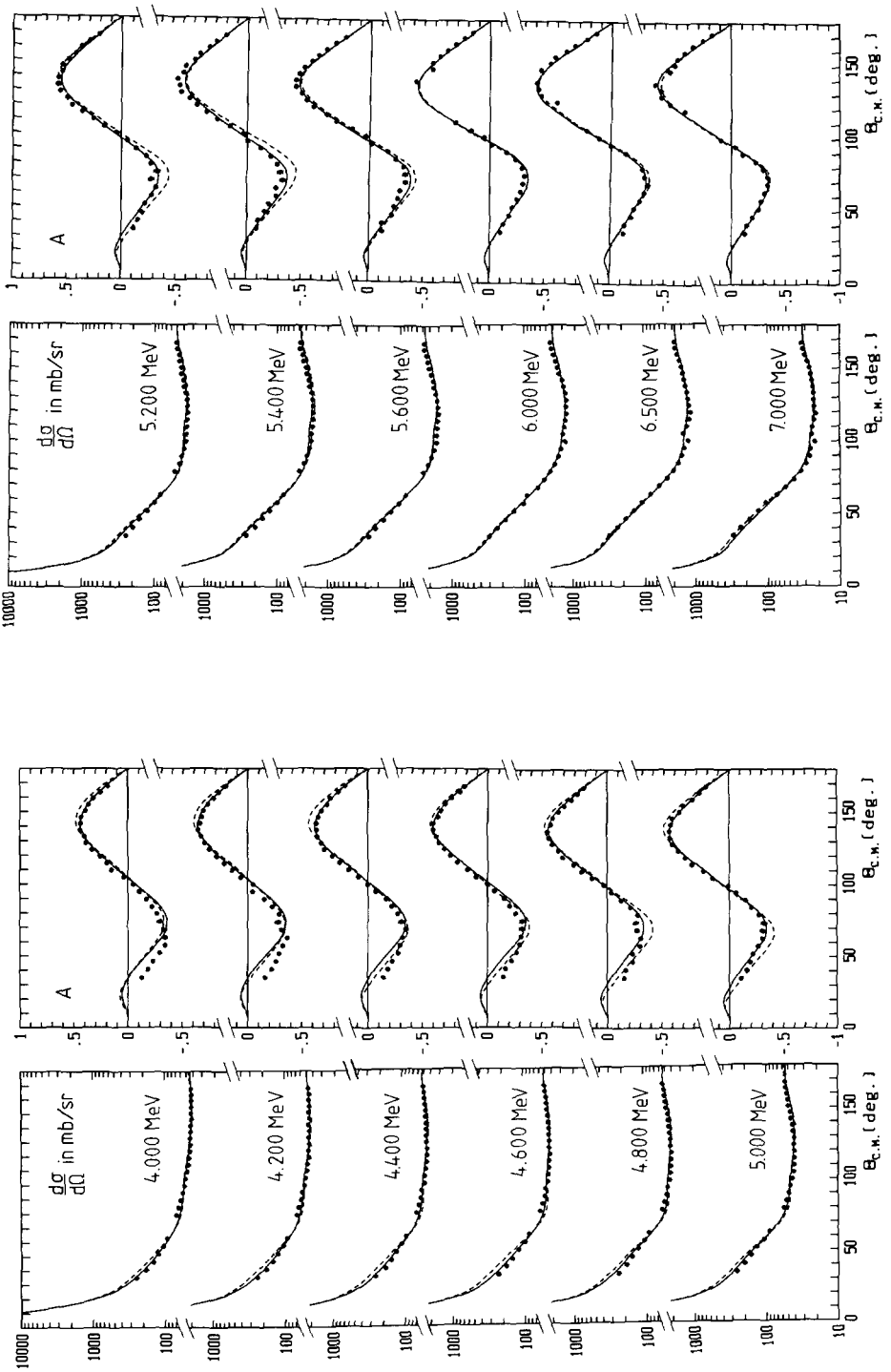

Fig. 5—continued

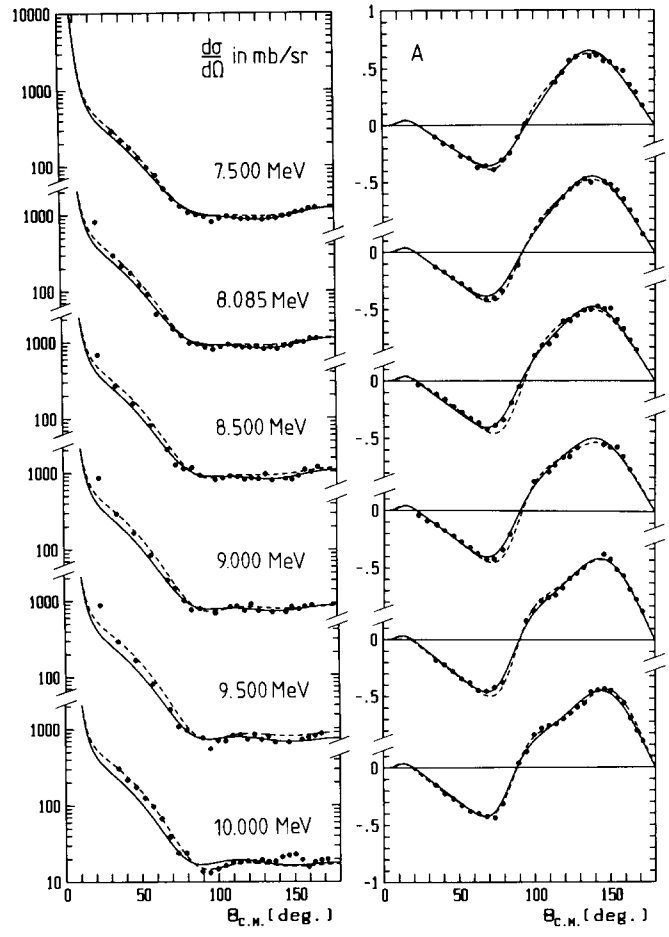

Fig. 5—continued

The volume integrals:

$$J_V/A = -\frac{1}{A}\int V(r)\,\mathrm{d}^3r = V_{03}^4\pi r_0^3\left[1+\left(\frac{\pi a_0}{r_0 A^{1/3}}\right)^2\right],$$

$$J_W/A = -\frac{1}{A}\int W(r)\,\mathrm{d}^3r = \frac{16\pi}{A^{1/3}}\,r_1^2 W_D a_1\left[1+\frac{1}{3}\left(\frac{\pi a_1}{r_1 A^{1/3}}\right)^2\right]$$

(A = mass number).

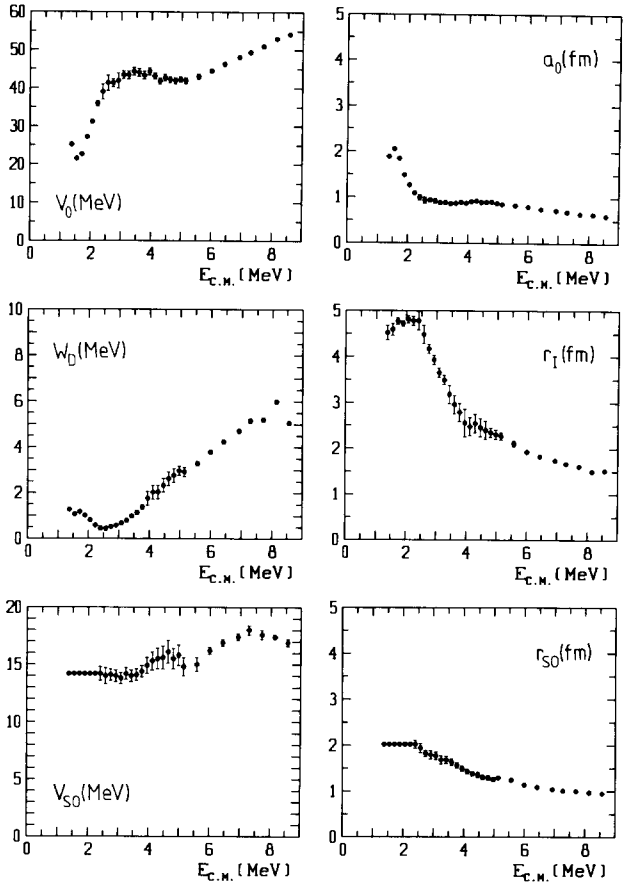

Fig. 6. Fitted optical-model parameters of procedure (I) (see text). The spin-orbit parameters were kept fixed below 2.4 MeV c.m. energy.

The mean square radii:

$$\langle R_V^2\rangle = \frac{\int V(r) r^2 \, \mathrm{d}^3 r}{V(r)\, \mathrm{d}^3 r} = \tfrac{5}{3} r_0^2 A^{2/3}\left[1+\frac{7}{3}\left(\frac{\pi a_0}{r_0 A^{1/3}}\right)^2\right],$$

$$\langle R_W^2\rangle = \frac{\int W(r) r^2 \, \mathrm{d}^3 r}{W(r)\, \mathrm{d}^3 r} = r_1^2 A^{2/3}\left[1+\frac{5}{3}\left(\frac{\pi a_1}{r_1 A^{1/3}}\right)^2\right].$$

The calculated values, corresponding to procedure (III), are given in figs. 9 and 10, respectively. They are compared to a Coulomb-corrected (according to ref. [11])) analysis of neutron scattering at ^{6}Li [ref. [4])], extrapolated to the energy region of

TABLE 1

Optical-model parameters of procedure (II) (see text), depending linearly on the lab energy E

r_C	1.25 fm (not varied)
V_0	3.80 MeV
r_0	1.40 fm
a_0	$1.02\ \text{fm} - 0.0479\ \frac{\text{fm}}{\text{MeV}} \times E$
W_D	$0.507 \times E$
r_I	$2.92\ \text{fm} - 0.135\ \frac{\text{fm}}{\text{MeV}} \times E$
a_I	0.404 fm
$V_{s.o.}$	$16.1\ \text{MeV} - 0.131 \times E$
$r_{s.o.}$	$1.88\ \text{fm} - 0.0887\ \frac{\text{fm}}{\text{MeV}} \times E$
$a_{s.o.}$	0.390 fm

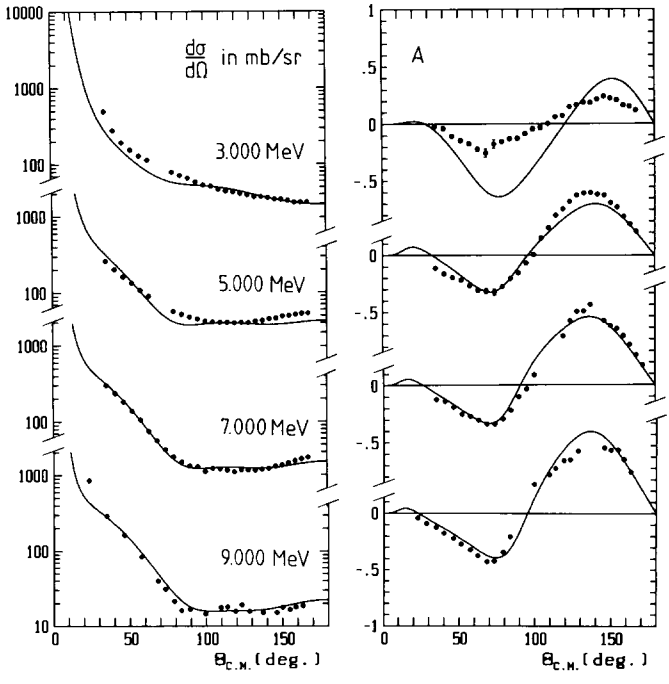

Fig. 7. Description of data through optical-model fit (II) (see text) at 3, 5, 7 and 9 MeV lab energy, using linearly energy-dependent parameters.

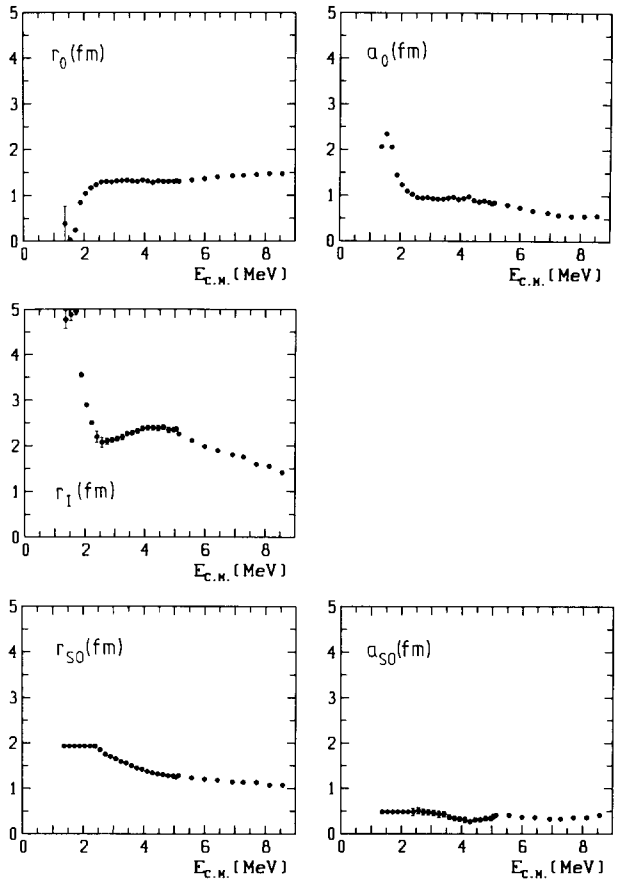

Fig. 8. Fitted optical-model parameters of procedure (III) (see text). The spin-orbit parameters were kept fixed below 2.4 MeV c.m. energy.

this work, and with the predictions of the microscopic model [5]) according to Jeukenne, Lejeune and Mahaux (JLM). Apart from the resonances, the magnitude of the volume integrals and the root mean square radii of our proton-scattering analysis agree both with the results of the neutron scattering and the JLM predictions. Because of the applied local-density approximation, the validity of the JLM model was originally restricted to mass numbers $A \geq 12$. Although $A = 6$ for ^{6}Li(p, p), the application of the JLM model seems practicable if we neglect resonance effects. These effects are not present in JLM nor in the neutron-scattering analysis, where all optical-model parameters are linearly energy dependent.

The unpolarized cross section of elastic neutron-scattering at various target nuclei from ^{6}Li to ^{13}C, in the energy range between 7 and 15 MeV, has been analyzed by Dave *et al.* [4]). In that analysis, unpolarized neutron data have been described with

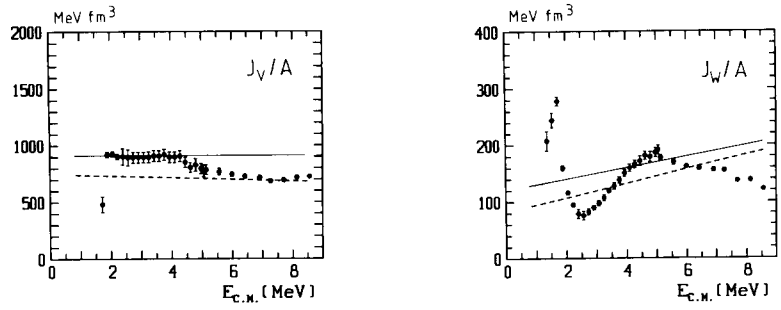

Fig. 9. Real and imaginary volume integrals per mass unit, calculated from the parameters of procedure (III) (see fig. 8). The solid curves belong to a neutron-scattering analysis [4]), they are Coulomb corrected and extrapolated to the corresponding energy range. The dashed curves show the prediction of the JLM model [5]).

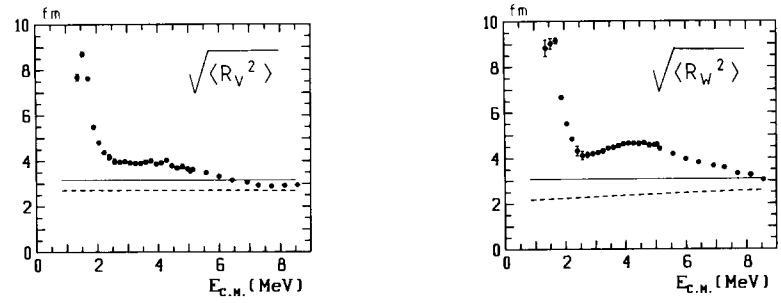

Fig. 10. Real and imaginary root mean square radii, calculated from the parameters of procedure (III) (see fig. 8). The curves are the same as in fig. 9.

linearly energy-dependent potential depths and constant geometry parameters, although the description was, according to the authors, not as good as for heavier nuclei, especially in regions of resonances. For our proton scattering analysis, however, both cross section and analyzing power could not be described simultaneously with constant geometry parameters, even if all potential depths were adjusted. As pointed out in ref. [4]), the parameter set from neutron scattering can also describe the unpolarized ^{6}Li(p, p) cross sections of ref. [12]) after applying a Coulomb correction by adjusting V_0 and W_D. This parameter set could not, however, describe our data [13]), with discrepancies mainly in the analyzing power.

5. Conclusions

The cross section and analyzing power of ^{6}Li(p, p) scattering in the energy range between 1.6 and 10 MeV lab energy are well described by optical-model calculations.

The parameters do not, however, depend smoothly on energy, but show a strong peak at $E_{c.m.} = 1.6$ MeV, corresponding to a well-known resonance, and a broad structure at $E_{c.m.} = 4$–5 MeV, where further resonances are predicted (see the following paper). The same structures are found in the total elastic cross section (fig. 4).

These structures do not necessarily appear in an analysis of the unpolarized cross section alone (e.g. ref. [4])), which can be described with weakly energy-dependent optical-model parameters. The gross features of the integrated parameters of this work agree with the corresponding results of neutron scattering and with the predictions of the JLM model (see figs. 9 and 10). Additionally, they reveal the existence of resonance structures which prevent us from applying the optical model in the usual way. This new information could be only obtained by the inclusion of the analyzing power data.

References

1) J.N. Bahcall, W.F. Huebner, S.H. Lubow, P.D. Parker and R.K. Ulrich, Rev. Mod. Phys. **54** (1982) 767
2) H.M. Hofmann, Nucl. Phys. **A416** (1984) 363c
3) H.M. Hofmann, T. Mertelmeier and W. Zahn, Nucl. Phys. **A410** (1983) 208
4) J.H. Dave and C.R. Gould, Phys. Rev. **C28** (1983) 2212
5) J.-P. Jeukenne, A. Lejeune and C. Mahaux, Phys. Rev. **C16** (1977) 80
6) J.A. McCray, Phys. Rev. **130** (1963) 2034
7) W. Schuster, dissertation, Erlangen, 1982
8) H. Leeb, computer code GOMEL, Vienna 1983, unpublished
9) F.D. Becchetti Jr. and G.W. Greenlees, Phys. Rev. **182** (1969) 1190
10) G.W. Greenlees, G.J. Pyle and Y.C. Tang, Phys. Rev. **171** (1968) 1115
11) J. Rapaport, Phys. Lett. **B92** (1980) 233
12) W.D. Harrison and A.D. Whitehead, Phys. Rev. **132** (1963) 2607
13) M. Betz, Zulassungsarbeit, Erlangen, 1985